Intermittent and spatially heterogeneous single-particle dynamics close to colloidal gelation

Yongxiang Gao and Maria L. Kilfoil*
Department of Physics, McGill University, Montréal, Canada H3A 2T8

(Received 2 January 2008; revised manuscript received 2 September 2008; published 29 May 2009)

Dynamical heterogeneities exist ubiquitously in materials near a dynamical arrest transition, such as glass formation or gelation. Among the readily discernible features of heterogeneous dynamics is a non-Gaussian exponential component in the distribution of the constituent particle displacements that is not understood at the single-particle level. We present an experimental study of particle dynamics and self–van Hove functions $G_s(r,t)$ in a colloid-polymer system approaching gelation. We show experimental evidence, in the special case of a gelation transition, for exponentially distributed times for anomalously large displacements, and confirm that an exponential tail in G_s arises from rare events with associated Poisson statistics. We focus on the role of the anomalous large displacements and analyze their time scales, relating them to other time scales typically used to describe structural relaxation in gels and glasses: the time to cage breakup and the time for re-emergence of Fickian behavior at long times. Furthermore, we search for a structural origin of the dynamical heterogeneity. Various quantities characterizing local structure are examined. We found evidence of a strong correlation between local structure and local dynamics, in contrast to what has been found in supercooled liquids.

DOI: 10.1103/PhysRevE.79.051406 PACS number(s): 82.70.Dd, 82.70.Gg, 61.43.Fs

In conventional liquids, dynamical relaxation is achieved through continuous Brownian motion of particles. As the temperature of a liquid approaches that of the glass transition, the dynamics slow down by orders of magnitude with only a moderate decrease of temperature [1,2]. Meanwhile, an unmistakable phenomenon appears of widely distributed particle motions, across the constituent particle population [1] and over time for individual particles [3,4]. The heuristic picture is that a particle may vibrate in a cage formed by its neighbors most of the time and suddenly hop. Such spatial and temporal dynamical heterogeneities in the constituent particles give rise to non-Fickian behavior in a supercooled liquid.

Non-Fickian behavior has been measured and described in a wide variety of systems near a jamming transition, by a plateau observed in the mean squared displacement, and a second time scale for recovery of diffusion via the structural relaxation, considered to be the time for these cages to break up or the time for the self-intermediate scattering function to decay to $1/e$ of its initial value. Another less-understood manifestation is a non-Gaussian broad tail in the van Hove particle displacement distributions, $G_s(\Delta x,\tau)$, of exponential character. This broad tail has been reported in a nearly hard-sphere colloidal system in the supercooled liquid regime [5], a granular material on approach to the jamming transition [6], biological cells that exhibit soft glassy rheology [7] where the detailed shape of the tail was not discussed, and in a polymer gel [8]. One explanation for this in all these systems is that there is a rare hopping in the dynamics as described above at exponentially distributed times. Simulated supercooled liquid studies have indicated that the entire distribution needs not be exponential, as the part at short distances remains Gaussian type [9]; nevertheless for the previous work on supercooled colloidal liquids the entire distribution was assigned to a stretched exponential [5]. The possibility of crossover of the exponential component into a bimodal Gaussian behavior at very long times has been suggested [9,10] and has been observed by us in an attractive colloidal system [11], appearing as a narrow Gaussian at short distances and a clear separate broad Gaussian component at large distances.

Recently, a compelling model has been shown able to reproduce the broad tail in $G_s(\Delta x,\tau)$ for a wide range of systems close to the glass or jamming transition [12], including for our attractive colloidal system at intermediate times [13]. In this model, each particle samples between one narrow and one broad Gaussian distribution of possible step sizes, corresponding to vibrational motion and to "hops," respectively. Two different sampling rates of hops are considered, with the rate for the first hop smaller than that for subsequent hops, and both sampling rates are assumed to be exponentially distributed. However, the hop definition in this model has considerable shortcomings. It samples all length scales from a Gaussian distribution in which most of the statistical weight is carried by small steps. Even if a particle hops, it is very likely that the particle still moves with a small step. This inevitably weakens the role played by large hops in a crossover from exponential behavior to Gaussian that is suggested in simulation [9]. Despite the ubiquitous appearance of, and intense interest in, this exponential tail both experimentally and theoretically, surprisingly there has been no prior experimental work at the level of individual particle dynamics investigating the microscopic origin of the tail or its crossover to a Gaussian distribution at long time.

Aside from the non-Gaussian behavior of the self–van Hove correlation function [12], there are other anomalous behaviors arising from dynamical heterogeneity. For example, nonexponential decay of the density-density correlation function [1] and decoupling of diffusion from the structural relaxation [14] are commonly observed in systems approaching the dynamical arrest transition. Therefore, understanding dynamical heterogeneity is fundamentally important for understanding slow glassy dynamics.

*kilfoil@physics.mcgill.ca

Intuitively, one would expect a correlation between the system dynamics and structure. However, no dramatic change is found in the static structure as measured by the radial distribution function on approach to the glass transition, in contrast to the dramatic change in dynamics. The focus of the search for a structural origin for the dynamics has shifted to examining the relationship between subtle changes in the local structure and the local dynamics. This tantalizing idea has attracted the attention of both theorists and experimentalists.

Investigation of the correlation between local dynamics and local structure can be achieved easily in computer simulations, which store positions of each particle as a function of time. In a simulation of binary Lennard-Jones system close to the glass transition, indications were found that a particle's dynamics are correlated with its local potential, as mobile particles were found to sit in a shallower potential well even though the difference in potential is small [3]. Only a mild correlation between the local volume and local dynamics was observed in simulations of a glass-forming polymer melt [15,16]. Simulations on a supercooled liquid using an "isoconfigurational ensemble" [17], which isolates the dynamical effect on the dynamical heterogeneity, show a strong correlation between the average local potential and "dynamical propensity," the average squared displacements, at some typical time over many independent runs starting from the same equilibrium configuration [18]. This demonstrates that a particle's mobility is highly correlated with its initial environment, given that initially each particle has the same mobility statistically. In [19], the authors disagree with this interpretation and claim that dynamical heterogeneity is due to a dynamical effect rather than originating from structure. These authors randomly assign a velocity to particles with known dynamical propensities and investigate the relation between particle dynamics (squared displacements during a typical time scale) and dynamical propensity. Only a weak correlation between them is found. In contrast, recent molecular dynamics (MD) simulations of aluminum in the glass state clearly identified a strong relation between a particle's local density and its mobility [20]: statistically, those particles with a lower local density are more mobile as evidenced by their larger mean-squared displacements. The local-density distribution of the most mobile particles is also well separated from that of the most immobile ones and its peak position is lower.

Experimentally, it is a difficult task to probe the local structure and dynamics for atomic systems due to the limitations on length and time scales. In colloidal systems, confocal microscopy makes such an investigation possible in three dimensions (3D). Using such real-space imaging, cage rearrangements near the glass transition in a soft repulsive colloidal system were determined more likely to occur in a less dense region [21]. However, in the same system as well as another that is more hard-sphere-like, the relationship between microstructure and microdynamics was probed [16] with little success. Only mild correlation was observed between them. Both of these experimental studies suffered from poor resolution in 3D. It remains controversial whether dynamics have a structural basis in glass-forming liquids.

Recent molecular-dynamics simulations of an attractive colloidal system near a gel transition identify two populations of particles with distinct mobilities: the "slow" particles form a rigid network of particles with the "fast" particles on the surface of the network where they tend to replace one another [22,23]. Despite the recent effort in understanding gels and glasses under the same glass paradigm [24,25], there have been very few experimental measurements of the dynamical heterogeneity in colloidal gels [11,13,26,27]. A recent confocal microscopy study of a polymer-induced depletion colloidal gel provides direct evidence of a link between local structure measured using a novel topological method and dynamical arrest [28]. Despite the insights gained into the nature of the gel transition via the focus on local structure, this work also suffers from poor 3D coordinate resolution and coordinate tracking errors that confound accurate measurements of the individual particle dynamics [28].

In this paper, we observe directly the intermittent hopping events at the level of individual particle dynamics. We do this in a colloidal model system using high-resolution particle dynamics data extracted by confocal fluorescence microscopy at controlled time intervals. Long times are accessed in the experiments during the approach to colloidal gelation using specialized tracking techniques to resolve the dynamics of all of the particles in the face of heterogeneous dynamics [29]. We define the hopping steps that give rise to the broad exponentially decaying component of the self–van Hove function in our system over a broad range of colloid volume fractions and time scales. We associate this hopping with cage breakup and the re-emergence of Fickian behavior at long times. Moreover, we investigate the relation between individual particle mobility and local environment to search for the origin of dynamical heterogeneity. The results suggest that the dynamics in attractive colloidal system have a more heterogeneous nature and a much stronger correlation with local structure compared to the dynamics in supercooled liquids.

We use an attraction-driven colloidal system formed at a low-to-moderate interparticle attraction strength described in [11]. The colloids are fluorescently labeled polymethylmethacrylate (PMMA) spheres of diameter 1.33 μm sitting in a solvent mixture of decahydronaphthalene (decalin), tetrahydronaphthalene (tetralin), and cyclohexyl bromide (CXB) designed to avoid the problem of charging that plagued previous studies employing decalin and cycloheptyl bromide (CHB), and that allows for independent matching of relative refractive index and buoyancy of the particles. Linear polystyrene polymer with radius of gyration 92 nm is added to induce an interparticle attraction of strength $2.86k_BT$ at contact via depletion. The small buoyancy mismatch $\Delta\rho=0.011$ mg/ml allows for a slow quench due to the increase in the particle volume fraction while the interaction strength and steric hindrance govern the microscopic dynamics. We use confocal microscopy to acquire stacks of images at 0.2 μm spacing in z at controlled time intervals ranging from 12 to 1500 s at different ϕ to access short- and long-time dynamics during the approach to gelation. The imaging volume is $(22.6\times22.6\times10)$ μm^3, containing approximately 2000 particles. We extract all the particle posi-

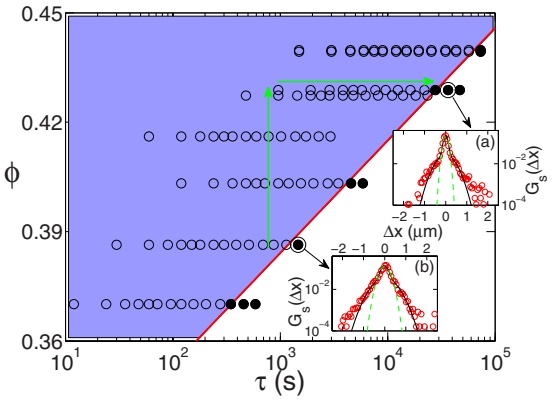

FIG. 1. (Color online) Diagram for region of $\phi-\tau$ space indicating the crossover from exponential to bimodal Gaussian distributions for the broad tails in the displacement distribution. Blue (shaded) region indicates the parameter space region over which the broad tail of $G_s(\Delta x,\tau)$ decays exponentially. Red (gray) solid line indicates the emergence of the broad Gaussian distribution for the broad tails in G_s. Symbols indicate the phase position of our data. Open symbols: exponential tails; solid symbols: Gaussian tails. Inset: (a) $G_s(\Delta x)$ for $\phi=0.429$ at $\tau=41280$ s; (b) $G_s(\Delta x)$ for $\phi=0.386$ at $\tau=1350$ s. Black solid line: bimodal Gaussian fit; green (light gray) dashed line: single Gaussian fit.

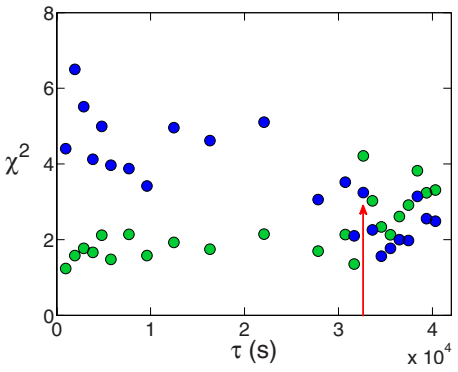

FIG. 2. (Color online) The least-squares χ^2 for Gaussian and exponential fits to the broad tails in $G_s(\Delta x,\tau)$ at $\phi=0.429$. Blue (dark gray) circles: least square of exponential fit; green (medium gray) circles: least square of Gaussian fit. Arrow indicates where the distribution crosses over from being better described by an exponential distribution to a Gaussian distribution the better fit.

tions at a resolution of better than 11 nm in three dimensions, determined by direct comparison of the performance of all the localization methods for colloids that achieve subpixel 3D resolution in [29], and track them over time to investigate the microscopic dynamics [29,30]. The gelation transition is at $\phi=0.442$ [11].

The self part of the van Hove correlation function $G_s(\Delta r,\tau)$ measures the probability of a particle excursion during a lag time τ [31]. The one-dimensional (1D) form, $G_s(\Delta x,\tau)=1/N\Sigma_{i=1}^{N}\delta[x+x_i(0)-x_i(\tau)]$, is symmetric and greater sensitivity to the experimental data is obtained by fitting the data to this form. In the following we present result solely for x. We have carried out the same analysis for y and z and the results are similar. This distribution provides a direct measure of the dynamical behavior of a system. It takes on a Gaussian shape for Fickian behavior. In our system, this distribution has a narrow peak with broad tails and cannot be described by a single Gaussian. We find that the broad tail itself is purely exponential over a wide range of ϕ and τ before it crosses over to a Gaussian at very long times, as shown in Fig. 1. The crossover is identified as the point when a Gaussian form fits the broad tail better than an exponential form based on the least squares of these two fits, as shown in Fig. 2.

In the insets of Fig. 1, we show two examples of the distribution taking the shape of a bimodal Gaussian at long time. The crossover to bimodal Gaussian at long times suggests the existence of two populations with distinctly different mobilities. In previous work, we used this long-time crossover to segregate the two populations [11]. We rank-ordered particles by their average step size in x. The fast particles were identified by requiring that the width of the $G_s(\Delta x,\tau)$ of a subset of the most mobile particles match that of the broad component of the bimodal Gaussian at long time. The slow particles were identified from the immobile end of the ranking, requiring the width of their distribution to match that of the narrow component. We emphasize that the definition we use here for fast and slow emerges naturally, while all other definitions from experimental data used previously have been arbitrary [3,5,16] and not connected to a natural separation. Moreover, we have unprecedented resolution in three dimensions, and tracking that demonstrates that we access large hops that other methods miss [29]. The emergence of the broad Gaussian is based on a quantitative objective measure. Although data is necessarily poorer at longer lag times, because of our superior quality tracking, we nevertheless can attain nearly two decades in the probability distribution even at the very long lag times for the broad tail, where otherwise no, or scant, data would be obtained.

Here, we focus on the exponential tails exhibited at short and intermediate times in the $G_s(\Delta x,\tau)$. We use the two populations identified in the previous work [11] to investigate the origin of these tails. In Fig. 3, we show this correlation function computed from the data for a series of experiments along two paths: constant ϕ and constant τ. We plot $G_s(\Delta x,\tau)$ for the entire population at $\phi=0.429$ over different lag times in Fig. 3(a). The prominent feature is a pronounced tail extending to distances that are much larger than expected for a Gaussian prediction. The broad tail can be fully described by a purely exponentially decaying function.

The distributions at different lag times can be normalized together by the exponential fit parameters [Fig. 3(c)]. In Fig. 3(b), we show results along constant lag time τ for different volume fractions. The broad tail in $G_s(\Delta x,\tau)$ becomes narrower due to the slowing down of the dynamics as ϕ is increased on the approach to the colloidal gel transition, while the central quasi-Gaussian peak becomes more prominent as a larger proportion of particles becomes sluggish. For constant τ at different ϕ, the broad tails can also be scaled together, aside from the narrow peak, as shown in Fig. 3(d). Both scalings show that the broad tail can be described by the same purely exponential functional form across a wide range of ϕ and τ for the entire shaded region in Fig. 1. This observation has motivated a theoretical investigation on the

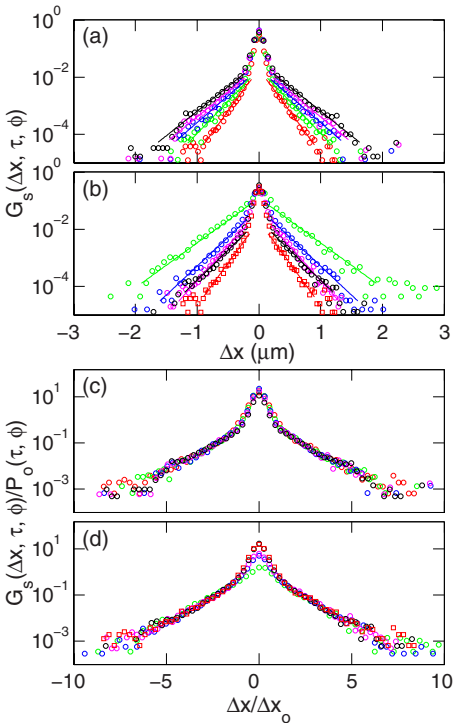

FIG. 3. (Color online) $G_s(\Delta x, \tau)$ for the entire population in (a) at ϕ=0.429 over, from innermost to outermost distributions, τ =960 s (red), 1920 s (green), 2880 s (blue), 4800 s (magenta), and 9600 s (black) and in (b) from broadest to narrowest distribution at the wings at τ=960 s for ϕ=0.386 (green), 0.403 (blue), 0.416 (magenta), 0.427 (black), and 0.429 (red). The solid lines in (a) and (b) are exponential fits for each data set $P(\Delta x, \tau)$ $=P_0 \exp(-|\Delta x|/x_0)$, where P_0 and x_0 vary in (a) with different τ and in (b) with ϕ. (c) and (d) are the same data as in (a) and (b), respectively, with x and P scaled by x_0 and P_0.

collapse of the exponential tails in dense hard-sphere systems, where it is predicted that the superposition of exponential tails holds as the packing volume fraction approaches that of the glass transition [32].

To investigate the origin of these tails, we examine the individual particle dynamics. In Fig. 4, we show some typical one-dimensional trajectories at different volume fractions for both fast and slow particles. The slow particles essentially have only small vibrational motion. In contrast, the fast particles have many more large displacements separated by small vibrational motions. In Fig. 5, we plot the instantaneous one-dimensional displacements derived from the raw trajectories of Fig. 4. As the volume fraction increases, longer time is required for particles to undergo approximately the same number of large displacements.

The evident difference between the mobilities of fast and slow particles motivates us to examine $G_s(\Delta x, \tau)$ for the two populations separately. We show the result for ϕ=0.440 in the inset of Fig. 6. The contributions to $G_s(\Delta x, \tau)$ from the fast and slow particles are overlain on $G_s(\Delta x, \tau)$ for all the particles. Clearly, the overwhelming contribution to the broad tail in the parent distribution is from the fast population, with the contribution from the slow particles at least 1 order of magnitude smaller. This observation holds for all volume fractions and lag times. To gain insight into the ac-

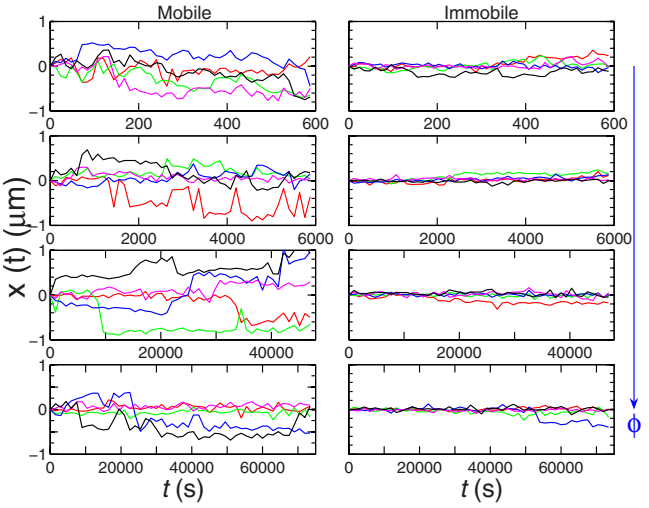

FIG. 4. (Color online) Typical experimental time traces for 1D (x) trajectories, plotted for fast (left panel) and slow (right panel) populations at four different volume fractions: from top to bottom, 0.370, 0.403, 0.429, and 0.440. Δt between successive time points are 12, 120, 960, and 1500 s from top to bottom.

tual displacements giving rise to the exponential tails, we plot a single distribution for the fast population alone in Fig. 6. It too is comprised of a nearly Gaussian central peak and a broad exponentially decaying tail, indicating that the fast population has both harmonic vibrational motion and large displacements that give rise to the exponential tails in the parent distribution.

To investigate the temporally heterogeneous dynamics of single particles, we define an intermittent event—a hop—as any displacement in the shortest time step (the sampling rate) with magnitude greater than a threshold x_{cut}. We use x_{cut} =0.1 μm, a natural choice for several reasons. First, x_{cut} =0.1 μm is approximately $2R_g/\sqrt{3}$, the bonding or localiza-

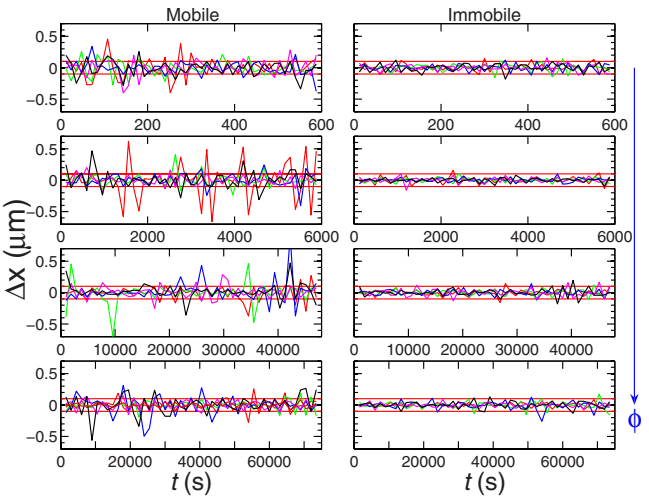

FIG. 5. (Color online) Typical magnitude of 1D displacement as a function of time for fast (left panel) and slow particles (right panel) corresponding to the raw x trajectories plotted above at four different volume fractions. The volume fractions and Δt between successive time points from top to bottom are as in Fig. 4. Solid red (gray) lines in each figure indicate where $|\Delta x|$=0.1 μm.

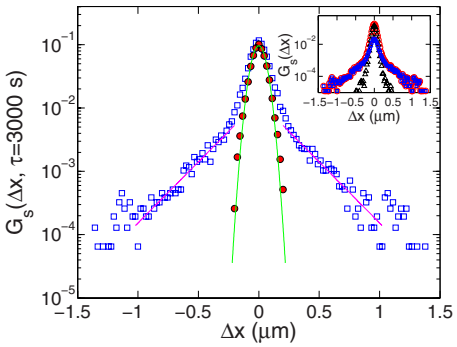

FIG. 6. (Color online) $G_s(\Delta x,\tau)$ for the fast population before (open blue squares) and after (filled red circles) removal of hops $|\Delta x| \geq 0.1$ μm (frame to frame distance larger than 0.1 μm) at $\phi=0.440$ and at a time scale $\tau=3000$ s, longer than the shortest τ. Purple (medium gray) line: exponential fit to the tail, $P(\Delta x,\tau)=P_0\exp(-|\Delta x|/x_0)$, with $x_0=0.225$ μm; green (light gray) line: Gaussian fit to the vibrational component, $P(\Delta x,\tau)\propto\exp[-(\Delta x)^2/2\sigma^2]$, with $\sigma=0.056$ μm. Inset: $G_s(\Delta x,\tau=3000$ s) for the entire population (red circles), the fast population (blue squares) and the slow population (black triangles) at $\phi=0.440$.

tion length one expects theoretically for one dimension in an attraction-driven colloidal system approaching an arrested transition [25]. Second, after removal of displacements larger than $x_{\rm cut}=0.1$ μm from $G_s(\Delta x,\tau)$ at the shortest τ (for the case shown in Fig. 6, $\tau=1500$ s), the remaining motion in the intervening time between hops is a harmonic vibration in the cage formed by neighboring particles (shown in Fig. 6). This also demonstrates that the exponential tails arise from those large hops. Third, by examining the 1D displacement trajectories shown in Fig. 5, small vibrational motion is bounded by this cutoff for slow particles, for which hops are very rare. Finally, the characteristic hopping time extracted below for the slow particles is close to the t_s^* we measured later for that population—the time scale when the non-Gaussian parameter shows a peak. The time scale t_s^* is at the end of the plateau in mean squared displacement and it is often interpreted as the time for cage breakup for repulsive glasses [5,33] or, for an attraction-driven glass, the bond breakage time. This is internally consistent with our heuristic picture for the definition of a hop.

To gain insight into the temporal heterogeneity, we measure the time between successive hops, illustrated for a typical trajectory in Fig. 7(a), and compute from the particle trajectories the probability distributions of the hop time scales for the fast and slow populations separately. The distribution is exponential, for both populations, for each ϕ. We show in Figs. 7(b) and 7(c) only the results at $\phi=0.386$ for fast and slow populations separately. Interestingly, such an exponential distribution of hop time scales is assumed in a continuous time random-walk (CTRW) model used to predict the exponential tail in $G_s(\Delta x,\tau)$ [12,13] and is in agreement with a prediction given by a nonlinear Langevin theory for activated dynamics [32]. To test whether there are variations in the dynamics during the course of the experiment, we have split our time series experimental data in half and measured both $G_s(\Delta x,\tau)$ and the distribution of the hopping times for each half. We find no difference in both quantities

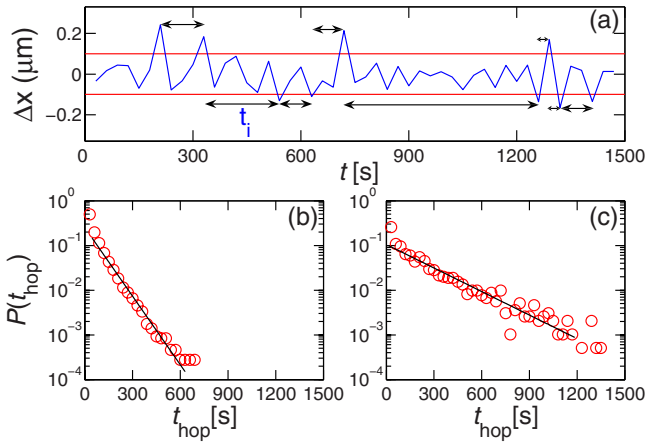

FIG. 7. (Color online) (a) Definition of hop time, demonstrated using the experimental time trace of 1D displacements for a typical fast particle. Solid red (gray) lines indicate where $|\Delta x|=0.1$ μm. Probability distribution of hopping time scales for (b) 10 788 hops of the fast population and for (c) 1954 hops of the slow population at $\phi=0.386$. Solid lines are fits to $P(t_{\rm hop})\propto\exp(-t_{\rm hop}/\tau_0)$ with first moments $\tau_0=84.7$ s for fast population and $\tau_0=247.5$ s for slow population at this ϕ.

between the first half, the second half, and the entire trajectory.

To examine the behavior of time scales as the system approaches the gel transition, where the dynamics become increasingly sluggish, we plot the characteristic hopping times for the segregated fast and slow populations against ϕ in Fig. 8. The characteristic hopping times all increase exponentially with ϕ. We find for other cutoff choices of $x_{\rm cut}=0.2$, 0.15, 0.12, and 0.075 μm that the hopping time scales all show similar ϕ dependence, with the actual frequency of hops decreasing with increasing $x_{\rm cut}$ and the time scale becoming inaccessible for the slow particles.

To interpret these times in the context of the time scale for structural relaxation, in Fig. 8 we also plot for the slow particles τ^*, the time at which the dynamics are most non-Gaussian and recovery of Fickian motion begins. We find

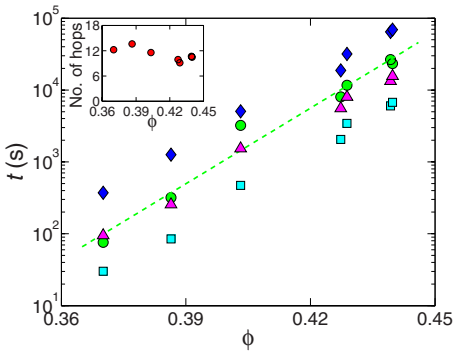

FIG. 8. (Color online) Hopping time scales vs ϕ. Squares: τ_0 of fast particles; triangles: τ_0 of slow particles; diamonds: time for emergence of bimodal Gaussian in $G_s(\Delta x,\tau)$; circles: τ^* of slow particles. Dashed line is exponential fit for τ^*. Inset: average number of hops undertaken by fast particles prior to emergence of bimodal Gaussian $G_s(\Delta x,\tau)$, plotted vs ϕ.

that τ^* is very close to the characteristic time, τ_0, of this slow population. This seems to endow τ^* with the physical meaning of the time scale for "cage" breakup to occur, where the cage here is the collective potential well of the nearest-neighbor particles.

In order to understand the relation between these times and the evolution of $G_s(\Delta x, \tau)$, we also plot in Fig. 8 the time scale for the emergence of the bimodal Gaussian distribution at very long times. It is longer than all the other times and also scales exponentially with ϕ, suggesting that the crossover time is a multiple of any of the hopping times. Since the fast particles dominate the exponential tail, we count the number of hops the fast particles undergo on average during this long time scale. These counts are plotted in the inset of Fig. 8. On average, the same number of anomalously large displacements are required, ~11, across all volume fractions. This suggests that the crossover to bimodal Gaussian in $G_s(\Delta x, \tau)$ in this system is as implied by the central limit theorem of probability theory. At short time those particles that are likely to hop have undergone only a few of these rare events, thus the hops obey Poisson statistics and the distribution is exponential. By contrast, at longer time those particles sample more large hops and the broad distribution becomes a Gaussian.

Since the broad tails in $G_s(\Delta x, \tau)$ are always ascribed to anomalously large displacements in other systems close to glass or jamming transitions as well, it would be very interesting to apply the same analysis on particle trajectories or the statistics of displacements to those systems. However, different behaviors may be expected. The crossover to bimodal Gaussian behavior may be unique to systems with attractive interactions because the two populations apparently remain largely separated throughout the very long experimental time window accessed here: the same set of data for the fast population reproduces the broad tails during the entire experimental time. Recently, a close interaction between experiments and simulations shows that gelation is a dynamically arrested state triggered by the equilibrium liquid-gas phase separation [34], which might be the reason for the emergence of the broad Gaussian distribution. Other systems with noninteracting particles, such as supercooled hard spheres and jammed granular systems, may never cross over to two Gaussian distributions on the time scale of the experiment, even over the very long time scales accessed here, because there will be exchange of particles as the dynamical heterogeneities visit all regions in space. There, the exponential tails would eventually disappear, but only when all the particles have undergone enough large displacements to cross over to Gaussian distribution. The G_s would therefore cross over to a Gaussian only upon recovery of Fickian behavior for the entire population [32]. There is also evidence for the difference between colloidal systems with attractions and other systems upon approach to the arrested transition when applying the CTRW model to our attraction-driven colloidal data [13]. The hop length scale and the vibrational length scale extracted from the model fit are much more separated, present at a ratio of ~4.7 at the highest volume fraction compared to ~2 in other noninteracting or Lennard-Jones systems [12]. This at least reflects that the dynamics exhibit greater heterogeneity in our system. Nevertheless, emergence of a bimodal Gaussian distribution has been observed in simulations of supercooled liquids using Lennard-Jones potential [9]. Whether a bimodal Gaussian will emerge in these other systems awaits experimental study.

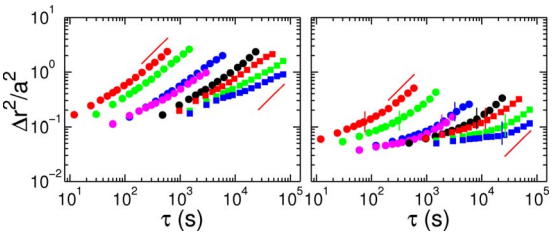

FIG. 9. (Color online) Mean-squared displacements for fast (left panel) and slow (right panel) populations segregated for volume fraction of 0.370 [red (leftmost) circles], 0.386 [green (light gray) circles], 0.403 [blue (dark gray) circles], 0.416 [magenta (medium gray) circles], 0.427 [black circles], 0.429 [red (medium gray) squares], 0.439 [green (light gray) squares], and 0.440 [blue (dark gray) squares]. Red (gray) solid lines delineate slope of 1, corresponding to purely diffusive behavior. The time scale of the peak in the non-Gaussian parameter has been marked by vertical lines for the slow population (right panel).

In Fig. 9, we show the ensemble-averaged mean-squared displacements (MSD) for the fast and slow populations separately. The dynamics become more sluggish as the volume fraction is increased for both the fast and slow populations. Qualitatively, close to the gel transition, the dynamics of slow particles become more subdiffusive and the plateau in MSD gets more prominent, a hallmark of approach to the glass or jamming transition. In contrast, the fast population shows nearly diffusive or merely subdiffusive behavior for all volume fractions. Quantitatively, we observe that the dynamics of the fast particles are approximately 1 order of magnitude faster than the dynamics of the slow particles at the corresponding volume fraction, as shown in Fig. 9.

To quantify the degree of deviation of the dynamical behavior of the slow particles from Fickian diffusion, we measure the classical non-Gaussian parameter (NGP), $\alpha_2(\tau) = \langle \Delta x^4(\tau) \rangle / (3\langle \Delta x^2(\tau) \rangle^2) - 1$ [35]. In a supercooled liquid, $\alpha_2(\tau)$ is zero at short time simply because the velocity distribution is a Maxwell distribution before any collisions occur. At intermediate times, a particle's motion is hindered by its neighbors. Some particles can escape from the cages formed by their neighbors and may undergo one or more large jumps. This will give rise to a broad distribution of mobility (dynamical heterogeneity), causing the system's behavior deviate from Fickian and become non-Gaussian. At long time, after many collisions, the motion of a single particle is that of a random walk and its behavior becomes Fickian once again [36]. We observe in our system that the behavior of slow particles is close to Gaussian behavior at short and long times and at intermediate time, a peak in NGP emerges. The results are shown in Fig. 10. The peak positions of NGPs, indicated by τ_s^*, extend to longer time scale and the peak height becomes higher (except that for the highest volume fraction, which may already be across the gel transition) as the system becomes more crowded. The ex-

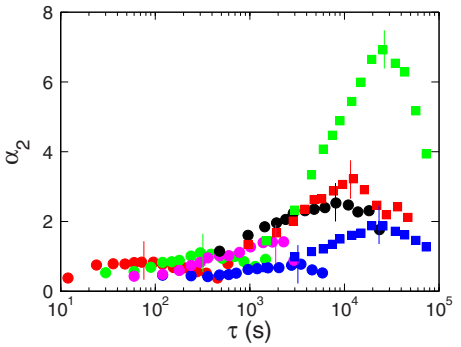

FIG. 10. (Color online) Non-Gaussian parameter $\alpha_2(\tau)$ computed of the slow population at volume fractions indicated by symbols as in Fig. 9. The time scale of the peak in the non-Gaussian parameter, marked by the vertical lines, is extracted.

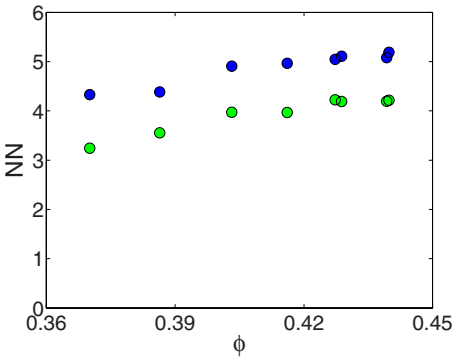

FIG. 11. (Color online) Average number of nearest neighbors for fast and slow particles separately. Blue (dark gray) symbols represent slow particles and green (light gray) symbols represent fast particles.

tracted τ_s^* is indicated by the vertical lines in the MSD of slow population, plotted for each volume fraction Fig. 9. For the volume fraction at which a plateau is observed in the MSD, τ_s^* is at the end of the plateau. This glasslike behavior of slow particles is reminiscent of the behavior observed by Manley *et al.* [37], who demonstrated that in colloidal gel, crowding in the colloid-rich region causes the dynamical arrest, much like in noninteracting hard spheres in the range of volume fractions $0.58 \leq \phi \leq 0.64$, the so-called hard-sphere glass regime. The plateau provides a localization length which reflects the cage size in repulsive glasses [33] and the "bond" length in attraction-driven glasses [38]. Usually, the localization length due to caging is considered to be roughly 10% of the particle diameter—the Lindemann criterion [25]. For our system, we expect the plateau height due to caging to occur at $\sim 0.04a^2$, while that due to bonding we expect to manifest at $\sim 0.08a^2$ [25], where a is the colloidal particle radius. The plateau we observe is at $\sim 0.07a^2$, sitting between the two theoretical values due to caging and bonding. Although the height of the plateau is much closer to the value predicted due to bonding, the mechanism for localization is still not completely unambiguous. The dynamical arrest could be caused by the caging effect or bonding, or possibly an interplay of both mechanisms, and merits further investigation using shorter range of attraction via confocal fluorescence microscopy.

To explain the drastically different dynamics we observe between the fast and slow populations, we make contact between a particle's mobility and its local environment. Intuitively, a particle's motion should be influenced by its local environment. Therefore, we expect a correlation between local dynamics and local structure. One of the simplest quantities to measure is the number of nearest neighbors, which we define as those particles located within the range of the potential for a given particle, since the resolution in the particle location in 3D is in our case 11 nm, less than the range of the depletion attraction we use. We calculate the number of nearest neighbors for fast and slow particles separately, averaged over the entire experimental time window. The results are presented in Fig. 11. We observe that on average, the slow particles have approximately one more nearest neighbor compared to the fast particles.

We gain further insight into the particles' local environments by calculating the local volume fraction ϕ_{loc} for each particle. We define ϕ_{loc} as the ratio of the volume of a particle to the volume of its Voronoi cell, the smallest polyhedron enclosing the particle whose faces are the planes that bisect imaginary center-to-center lines connecting a particle with each of its neighbors [39]. We perform Voronoi tessellation for all of the individual particles that are at least 1.8 μm away from the edge of the imaging volume, to avoid any edge effect, and verify this by examining the distribution of Voronoi volumes for all the particles at a given ϕ. The distribution shows no discernible changes as the distance from the edge is made larger than 1.8 μm. To avoid random time-dependent fluctuations of ϕ_{loc}, we use the average ϕ_{loc} over all time steps. Results for the distribution of ϕ_{loc} for fast and slow populations at different overall volume fractions are presented in Fig. 12. The peak position of the fitted distribution for the fast population is well separated from the peak of the distribution for the slow population, for experiments performed at all different global volume fractions, and is always lower. The results for the peak positions extracted from the ϕ_{loc} distributions are plotted for each ϕ in the inset of Fig. 12(c), which demonstrates that the slow particles have on average a higher ϕ_{loc} compared to the fast particles. Both the local-density analysis and the nearest-neighbor analysis therefore indicate a much stronger correlation between the microscopic dynamics and local environment than previously observed in nearly hard-sphere systems close to the glass transition [16]. Moreover, we observe that the local packing density increases for both fast and slow particles as the bulk volume fraction is increased. This strong correlation between local dynamics and local structure is in contrast to what was observed in dense colloidal systems without added attraction [16]. There might be fundamental a difference for this behavior between the attraction-driven and hard-sphere systems. However, it might also be caused by the significantly higher error in identifying particle positions, as well as what we believe, based on a direct test of tracking in the face of heterogeneous dynamics [29], to be the existence of a rather severe problem of missing tracks for the most mobile particles in particle tracking in the hard-sphere studies of [16]. Our methods in [29] demonstrate that much of the previous works in the field, based on less accurate ways of

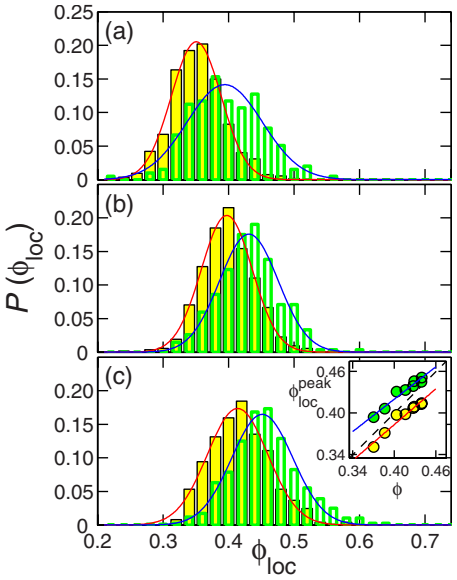

FIG. 12. (Color online) The probability distribution of averaged ϕ_{loc} over the entire experimental time for fast and slow particles separately for volume fractions (a) ϕ=0.370, (b) ϕ=0.403, and (c) ϕ=0.440. Yellow (filled) histogram represents the fast population; green (unfilled) histogram represents the slow population. Solid lines are Gaussian distribution fits to each distribution. Inset of (c): the peak position of the Gaussian distribution fit as a function of ϕ. Yellow (lower) circles: fast population; green (upper) circles: slow population. Red (lower) solid line indicates the linear fit to the data for the fast particles and blue (upper) solid line represents the fit for slow particles. Dashed line indicates ϕ, the bulk volume fraction.

determining particle dynamics, should be re-evaluated in light of the fact that physical phenomena identified may in fact simply reflect particle tracking artifacts.

We investigate dynamical heterogeneities at the typical time scale of τ_s^* using two different definitions for a particle's mobility: one is the end-to-end distance of the particle's trajectory over the time scale τ_s^* [21], illustrated in Fig. 13(a), and the other is defined as the particle's maximum displacement during the trajectory from its initial position at t=0 [3], illustrated in Fig. 13(b). We associate a color scheme to particle mobilities, as indicated by the scale in Fig. 13(e). We then construct spatial maps of dynamical heterogeneity for each definition. The results for the two definitions for ϕ =0.429 are shown in Figs. 13(c) and 13(d), respectively. Each snapshot is constructed based on 3D real-space data obtained by confocal microscopy. Unit vector arrows are placed on the most mobile particles to indicate the direction of motion. The length of the vector indicates out-of-plane or in-plane motion: the longer the vector, the greater the component of motion in plane. The heterogeneities revealed by the two definitions are quite similar. We find that the mobility, rather than being scattered randomly, tends to "nucleate." Closer to the gel transition, more and more particles become slow and the clusters of mobile particles shrink. Mobility is confined to increasingly localized regions, in reverse to the picture of melting, where the Lindemann criterion is exceeded in melting pockets. Although we observe some degree of correlated motion (over length scale on the order of

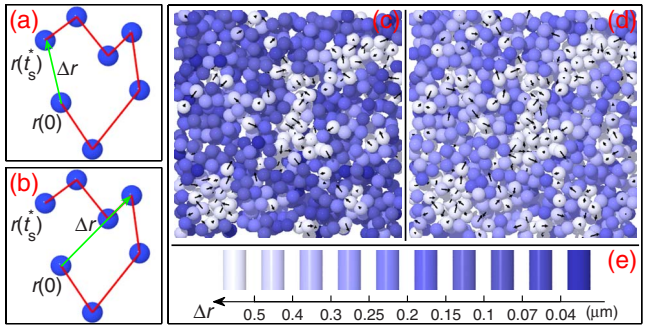

FIG. 13. (Color online) Comparison of dynamical heterogeneity for two different definitions of mobility. The mobility is ranked based on (a) the end-to-end distance traveled in t_s^* and (b) the maximum displacement from $r(t=0)$ over the interval t_s^*. Snapshots of dynamical heterogeneity based on the definitions in (a) and (b) are shown in (c) and (d), respectively, for ϕ=0.429. Unit length arrows are placed on those particles having displacements larger than 0.35 μm as two-dimensional (2D) projections of the unit vectors onto the x-y plane. (e) Mobility color map scale used for (c) and (d). The field of view for (c) and (d) is $(22.6\times22.6\times5)$ μm^3.

several particle diameters), we do not see the evident string-like motion that has been observed in supercooled liquids [3,33]. This may be due to the existence of large open space in the dense gels that does not have a counterpart in the hard-sphere glass that might interrupt the correlated motion.

We have investigated dynamical heterogeneities in an attractive colloidal system on approach to the gel transition. We have reported that purely exponentially distributed broad tails exist in the self–van Hove distribution over a broad range of times and ϕ close to the colloidal gel transition. We show that the tails are mainly due to rare and intermittent hopping events in the particle trajectories of the most mobile particles at exponentially distributed time intervals. The slow particles show dynamical behavior reminiscent of glasses obtained by the volume fraction route, lending support to the idea that colloidal gels and glasses can be considered under the same conceptual framework. There are nevertheless important differences observed: separable fast and slow components are not observed in hard-sphere glasses, most likely because the mobile regions in gels tend to nucleate around the voids that are a unique part of their structure. This is supported by the fact that we observe a much stronger correlation between microscopic structure and microscopic dynamics, examined at the level of single particles, than what has been observed in supercooled liquids of nearly hard spheres. Overall, slow particles have more neighbors than fast particles, consistent with our other observations that slow particles have a higher local volume fraction. Such information has never been revealed before and provides fundamental insight into the structural relaxation mechanisms in attraction-driven colloidal systems.

We thank Andrew Schofield and Peter Pusey of University of Edinburgh for providing PMMA latex particles. This work was supported by the Canadian Foundation for Innovation (CFI) and the Natural Sciences and Engineering Research Council of Canada (NSERC).

[1] M. D. Ediger, C. A. Angell, and S. R. Nagel, J. Phys. Chem. **100**, 13200 (1996).
[2] K. Binder and W. Kob, *Glassy Materials and Disordered Solids: An Introduction to Their Statistical Mechanics*, 1st ed. (World Scientific, Singapore, 2005).
[3] C. Donati, S. C. Glotzer, P. H. Poole, W. Kob, and S. J. Plimpton, Phys. Rev. E **60**, 3107 (1999).
[4] L. Cipelletti and L. Ramos, J. Phys.: Condens. Matter **17**, R253 (2005).
[5] E. R. Weeks, J. C. Crocker, A. C. Levitt, A. Schofield, and D. A. Weitz, Science **287**, 627 (2000).
[6] G. Marty and O. Dauchot, Phys. Rev. Lett. **94**, 015701 (2005).
[7] P. Bursac, G. Lenormand, B. Fabry, M. Oliver, D. A. Weitz, V. Viasnoff, J. P. Butler, and J. J. Fredberg, Nature Mater. **4**, 557 (2005).
[8] F. K. Oppong, L. Rubatat, B. J. Frisken, A. E. Bailey, and J. R. deBruyn, Phys. Rev. E **73**, 041405 (2006).
[9] D. A. Stariolo and G. Fabricius, J. Chem. Phys. **125**, 064505 (2006).
[10] P. I. Hurtado, L. Berthier, and W. Kob, Phys. Rev. Lett. **98**, 135503 (2007).
[11] Y. Gao and M. L. Kilfoil, Phys. Rev. Lett. **99**, 078301 (2007).
[12] P. Chaudhuri, L. Berthier, and W. Kob, Phys. Rev. Lett. **99**, 060604 (2007).
[13] P. Chaudhuri, Y. Gao, L. Berthier, M. Kilfoil, and W. Kob, J. Phys.: Condens. Matter **20**, 244126 (2008).
[14] S. C. Glotzer, J. Non-Cryst. Solids **274**, 342 (2000).
[15] F. W. Starr, S. Sastry, J. F. Douglas, and S. C. Glotzer, Phys. Rev. Lett. **89**, 125501 (2002).
[16] J. C. Conrad, F. W. Starr, and D. A. Weitz, J. Phys. Chem. B **109**, 21235 (2005).
[17] A. Widmer-Cooper, P. Harrowell, and H. Fynewever, Phys. Rev. Lett. **93**, 135701 (2004).
[18] G. S. Matharoo, M. S. Gulam Razul, and P. H. Poole, Phys. Rev. E **74**, 050502(R) (2006).
[19] L. Berthier and R. L. Jack, Phys. Rev. E **76**, 041509 (2007).
[20] M. Li, C. Z. Wang, M. I. Mendelev, and K. M. Ho, Phys. Rev. B **77**, 184202 (2008).
[21] E. R. Weeks and D. A. Weitz, Phys. Rev. Lett. **89**, 095704 (2002).
[22] A. M. Puertas, M. Fuchs, and M. E. Cates, J. Chem. Phys. **121**, 2813 (2004).
[23] A. M. Puertas, M. Fuchs, and M. E. Cates, J. Phys. Chem. B **109**, 6666 (2005).
[24] K. A. Dawson, Curr. Opin. Colloid Interface Sci. **7**, 218 (2002).
[25] F. Sciortino, Nature Mater. **1**, 145 (2002).
[26] C. J. Dibble, M. Kogan, and M. J. Solomon, Phys. Rev. E **74**, 041403 (2006).
[27] C. J. Dibble, M. Kogan, and M. J. Solomon, Phys. Rev. E **77**, 050401(R) (2008).
[28] C. P. Royall, S. R. Williams, T. Ohtsuka, and H. Tanaka, Nature Mater. **7**, 556 (2008).
[29] Y. Gao and M. L. Kilfoil, Opt. Express **17**, 4685 (2009).
[30] J. C. Crocker and D. G. Grier, J. Colloid Interface Sci. **179**, 298 (1996).
[31] A. Rahman, Phys. Rev. **136**, A405 (1964).
[32] E. J. Saltzman and K. S. Schweizer, Phys. Rev. E **77**, 051504 (2008).
[33] W. Kob, C. Donati, S. J. Plimpton, P. H. Poole, and S. C. Glotzer, Phys. Rev. Lett. **79**, 2827 (1997).
[34] P. J. Lu, E. Zaccarelli, F. Ciulla, A. B. Schofield, F. Sciortino, and D. A. Weitz, Nature (London) **453**, 499 (2008).
[35] B. R. A. Nijboer and A. Rahman, Physica **32**, 415 (1966).
[36] J. M. Haile, *Molecular Dynamics Simulation: Elementary Methods* (Wiley, New York, 1997).
[37] S. Manley, H. M. Wyss, K. Miyazaki, J. C. Conrad, V. Trappe, L. J. Kaufman, D. R. Reichman, and D. A. Weitz, Phys. Rev. Lett. **95**, 238302 (2005).
[38] K. N. Pham, A. M. Puertas, J. Bergenholtz, S. U. Egelhaaf, A. Moussaid, P. N. Pusey, A. B. Schofield, M. E. Cates, M. Fuchs, and W. C. K. Poon, Science **296**, 104 (2002).
[39] A. Rahman, J. Chem. Phys. **45**, 2585 (1966).